drones

Article

Prediction of Rice Brown Spot Disease Using Spectral Indices Derived from UAVs and Machine Learning Models in Lambayeque and Cajamarca, Peru

Juan Valdiviezo [1], Jaime Aguilar-Lome [2,*], María Jaramillo-Carrión [3], Luis Ángel Ruiz [4] and Lia Ramos-Fernández [5]

[1] Doctorado en Ingeniería y Ciencias Ambientales, Universidad Nacional Agraria La Molina, Lima 15024, Peru; 20240317@lamolina.edu.pe
[2] Laboratorio de Teledetección, Facultad de Ciencias Físicas, Universidad Nacional Mayor de San Marcos, Lima 15081, Peru
[3] Laboratorio de Fitopatologia, Universidad Nacional Pedro Ruiz Gallo, Lambayeque 14013, Peru; mjaramillo@unprg.edu.pe
[4] Geo-Environmental Cartography and Remote Sensing Group (CGAT), Universitat Politècnica de València, Camí de Vera s/n, 46022 Valencia, Spain; laruiz@cgf.upv.es
[5] Department of Water Resources, Universidad Nacional Agraria La Molina, Lima 15024, Peru; liarf@lamolina.edu.pe
* Correspondence: jaime.aguilar@unmsm.edu.pe

Highlights

What are the main findings?

- UAV-derived spectral variables were significantly associated with rice brown spot severity, with NDRE showing the strongest negative correlation (r = −0.83) and NPCI the strongest positive correlation (r = 0.77).
- Among the tested models, SVR-linear showed the slightly lowest prediction error for brown spot severity using NDRE, GREEN, and BLUE as predictors (R^2_CV = 0.76; RMSE_CV = 1.31).

What is the implication of the main finding?

- Multispectral UAV imagery can support plot-level estimation of rice brown spot severity under field conditions.
- Integrating UAV-derived spectral information with machine-learning models may improve disease monitoring and support future precision-management strategies in rice production.

Academic Editors: Pablo Rodríguez-Gonzálvez, Alexandre Maniçoba da Rosa Ferraz Jardim and Luciana Sandra Bastos De Souza

Received: 16 April 2026
Revised: 8 June 2026
Accepted: 26 June 2026
Published: 29 June 2026

Abstract

Rice brown spot, caused by *Bipolaris oryzae*, is an important constraint for rice production and requires timely field-scale monitoring. This study evaluated the use of multispectral bands acquired with a UAV-mounted sensor, together with vegetation indices, combined with machine-learning models to estimate rice brown spot severity under field conditions in Lambayeque and Cajamarca, Peru. A total of 37 sampling observations were collected across the vegetative, flowering, and milk-ripening stages. Spectral variables were extracted from UAV orthomosaics and related to field-based disease severity assessments. The strongest correlations with severity were observed for NDRE (r = −0.83) and NPCI (r = 0.77). Three regression models were evaluated using leave-one-out cross-validation (LOOCV): support vector regression with radial basis function kernel (SVR-rbf), support vector regression with linear kernel (SVR-linear), and Random Forest (RF). The SVR-linear model showed the lowest prediction error using NDRE, GREEN, and BLUE as predictors

 https://doi.org/10.3390/drones10070495

(R^2_CV = 0.76; RMSE_CV = 1.31), although its performance was very similar to that of SVR-rbf and RF. These results indicate that UAV-derived multispectral information can support plot-level estimation of rice brown spot severity. However, model performance should be interpreted cautiously because of the small dataset, heterogeneous disease conditions, and moderate prediction accuracy. Further studies with larger and independent datasets are needed to improve robustness and transferability.

Keywords: spores; rice brown spot; *Bipolaris oryzae*; UAV; machine learning; spectral indices

1. Introduction

In addition to adverse climatic conditions, diseases cause substantial losses in rice production [1]. Rice is one of the most important staple foods for the world's population; however, annual yield losses due to rice diseases range from 10 to 30% [2]. Therefore, the prediction and monitoring of rice diseases are essential not only to ensure crop quality and yield, but also to support food security for a large part of the global population [3]. Conventional large-scale disease monitoring methods are usually labor-intensive, time-consuming, spatially discontinuous and often lack precision. In this context, unmanned aerial vehicles (UAVs) can provide high-spatial-resolution information at the field scale and offer new opportunities for disease monitoring in agricultural systems.

UAV-based imagery, particularly multispectral data, has emerged as a useful tool for crop disease monitoring because it captures canopy-level spectral responses associated with plant stress. Different machine-learning approaches have been applied to detect and classify crop diseases using UAV data, and previous reviews have highlighted their potential for improving agricultural monitoring [4,5]. In rice, UAV- or satellite-based imagery combined with machine-learning approaches has been used mainly to detect or classify diseases such as rice blast, using spectral, textural, thermal, or combined features [6–13]. Although these studies differ from the present work in sensor type, target disease, and modeling objective, they provide useful methodological background on the use of image-derived variables and machine-learning approaches for rice disease assessment. The specific problem addressed in this study is the quantitative field-scale estimation of rice brown spot severity.

Brown spot disease, caused by *Bipolaris oryzae*, remains a relevant constraint for rice production because it affects leaf physiology, is associated with qualitative and quantitative crop damage, and may compromise grain filling under favorable epidemic conditions [14,15]. Previous studies have reported that *Bipolaris oryzae* infection can alter physiological and biochemical responses in rice plants, including pigment-related changes, which provide a biological basis for spectral disease assessment [16]. Hyperspectral studies have demonstrated that rice brown spot severity can be estimated from leaf- and canopy-level reflectance data, confirming that disease-induced changes are detectable in specific spectral regions [17,18]. However, these studies have mainly relied on proximal or hyperspectral measurements, which provide detailed spectral information but are less accessible for routine field-scale monitoring than UAV-derived multispectral imagery.

Although UAV- and machine-learning-based approaches have been increasingly used for rice disease monitoring, previous studies have focused on rice blast, general disease classification, or disease presence/absence detection [3,19–23]. Therefore, their direct applicability to quantitative brown spot severity estimation remains limited. In addition, spectral responses associated with disease should be interpreted within the broader context of crop stress, because vegetation indices derived from visible, red-edge, and near-infrared (NIR) bands are sensitive to changes in pigment concentration, canopy vigor, biomass,

https://doi.org/10.3390/drones10070495

and canopy structure, which may also be influenced by phenological stage, water or nutrient status, and crop management practices [24,25]. For this reason, UAV-derived spectral variables should be related to field-based disease assessment and phytopathological evidence rather than interpreted as disease-specific indicators by themselves.

Few studies have evaluated this problem under Peruvian field conditions, where disease expression, crop management, and environmental heterogeneity may differ from those reported in other rice-growing regions. The present study addresses this gap by evaluating the use of UAV-acquired multispectral imagery and derived vegetation indices for estimating field-assessed rice brown spot severity caused by *Bipolaris oryzae* under contrasting rice-producing environments in northern Peru. Therefore, the objective of this study was to estimate brown spot severity using spectral bands acquired with a UAV-mounted multispectral sensor and vegetation indices, and to compare the performance of SVR-rbf, SVR-linear, and RF models through leave-one-out cross-validation. Lambayeque and Cajamarca were selected as contrasting rice-producing environments in northern Peru, differing in agroecological setting, field conditions, and disease-establishment context.

2. Materials and Methods

2.1. Study Area

The research was carried out on two experimental plots: the first is located in the Paredones area (Figure 1c), in the District of Chongoyape, Province of Chiclayo, in the southeast of the Lambayeque Region at 6°37′20″ S and 79°22′8″ W at an altitude of 250 m above sea level. During the UAV surveys, the mean temperature was 22.3 °C and the relative humidity was 82%, as recorded by a portable ATMOS41 ZL6 model station. This area is characterized by a dry season from April to October and a rainy season from November to March. The second area is located in the Carhuaquero sector (Figure 1d), Cajamarca Region, at 6°27′30″ S and 79°12′03″ W at an altitude of 710 m above sea level, with a temperature of 24.7 °C and relative humidity of 82%. Both variables are averages of three dates on which the drone was flown. The study areas were selected to represent contrasting rice-producing environments in northern Peru and to ensure field feasibility through institutional collaboration and access to experimental and commercial rice plots.

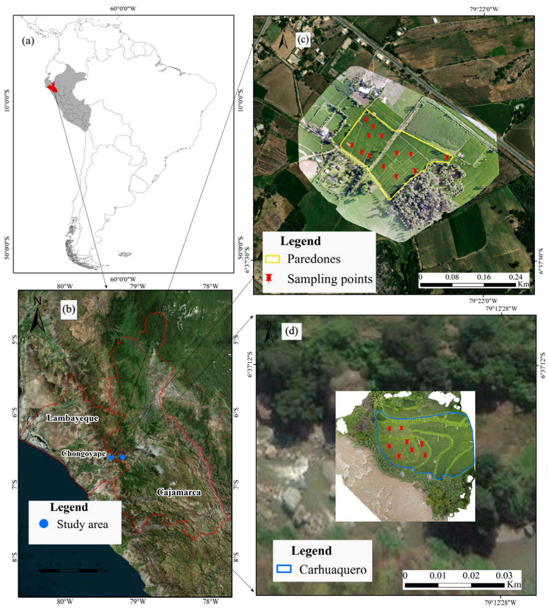

Figure 1. Study area: (**a**) Geographical location of Peru; (**b**) Lambayeque and Cajamarca regions; (**c**) rice-growing areas in Paredones and (**d**) Carhuaquero. The red pushpins indicate the location of the sampling points.

2.2. Field Data Collection

The experiment was conducted in rice fields planted with the *El Valor* variety. During each monitoring campaign, 1 m-high poles were installed in the rice fields. In total, 37 sampling observations were used in the analysis. These observations were obtained from 13 sampling posts evaluated once in Paredones during the flowering stage and eight sampling posts evaluated on three monitoring dates in Carhuaquero, corresponding to the vegetative, flowering, and milk-ripening stages. Thus, the dataset comprised 13 observations from Paredones and 24 observations from Carhuaquero, resulting in 37 sampling observations.

In Paredones, sampling points were established in a larger commercial rice field with an approximate area of 38,229 m^2, where the available space allowed the sampling points to be distributed across different parts of the field. In Carhuaquero, the experiment was conducted in a smaller field with an approximate area of 2741 m^2, and the sampling points were placed to avoid overlap between the 1 m-radius sampling areas used for leaf collection and spectral extraction. The layout was not a fully randomized experimental design; rather, sampling points were positioned according to accessibility, plot geometry, and the need to cover the spatial variability of crop canopy and disease occurrence. Therefore, the sampling design should be interpreted as a field-based spatial sampling scheme rather than a randomized block design.

The two sites differed in disease establishment conditions. In Paredones, a brown spot occurred under natural infection in a commercial rice field, whereas in Carhuaquero, artificial inoculation was used to ensure disease occurrence under a more controlled field setting. The datasets from both sites were combined because the objective was not to compare infection methods, but to develop regression models relating UAV-derived spectral variables to field-assessed brown spot severity across a broader range of disease conditions and phenological stages. In all cases, the response variable was the same disease severity score, and the presence of *Bipolaris oryzae* was supported by field symptom assessment, spore monitoring, and laboratory-based pathogen identification.

At the top of each 1 m-high pole, measured from the soil surface, a housing containing four microscope slides coated with glycerine was placed to allow airborne spores to adhere (Figure 2). The passive traps were installed close to the rice canopy to provide an integrated indication of airborne *Bipolaris oryzae* inoculum around each sampling point. Representative field photographs of the installed posts, passive spore traps, the surrounding leaf sampling area, and UAV flight setup are provided in Figure S3. In the Paredones sector, poles with spore traps were installed three days before the UAV flight, and the microscope slides were collected three days after the flight. In the Carhuaquero sector, the poles were installed six days before the UAV flight, and the slides were collected on the same day as the flight. These exposure periods were used to accumulate detectable airborne spores around the UAV monitoring window. Spore monitoring was used together with field symptom assessment and laboratory identification to support pathogen presence, while UAV-derived spectral variables were used to estimate field-assessed brown spot severity. Table 1 summarizes the inoculation and monitoring dates for field data collection at different phenological stages.

Table 1. Field monitoring schedule, inoculation condition, number of sampling posts, and phenological stage were evaluated in the Paredones and Carhuaquero sectors.

Sites	Inoculum Date	Post Installation Date	Flight Date	Slide Collection Date	Number of Posts	Phenological Stages
Paredones	Natural	16/04/25	19/04/25	22/04/25	13	Flowering
Carhuaquero	06 and 29/12/25	12/01/26	16/01/26	16/01/26	8	Vegetative
	04/02/26	04/02/26	10/02/26	20/02/26	8	Flowering
		20/02/26	26/02/26	27/02/26	8	Milk stage

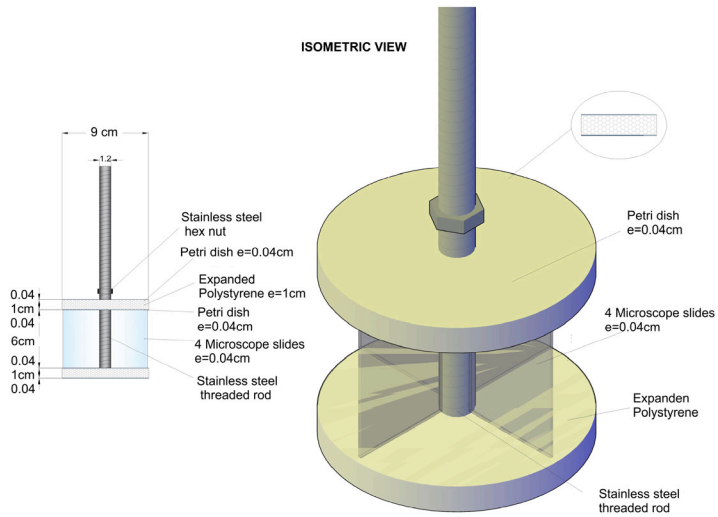

Figure 2. Spore-trapping device installed on 1 m-high poles in the rice field. The device contained four microscope slides coated with glycerine to collect airborne fungal spores.

After collection, the housing containing microscope slides was transported in a box to the Plant Pathology Laboratory at the Pedro Ruiz Gallo National University (UNPRG) for analysis. Fungal spore counts were performed using a Leica DM500 optical microscope (Leica, Heerbrugg, Switzerland). The number of spores found at each sampling point for each sector is shown in Figure 3.

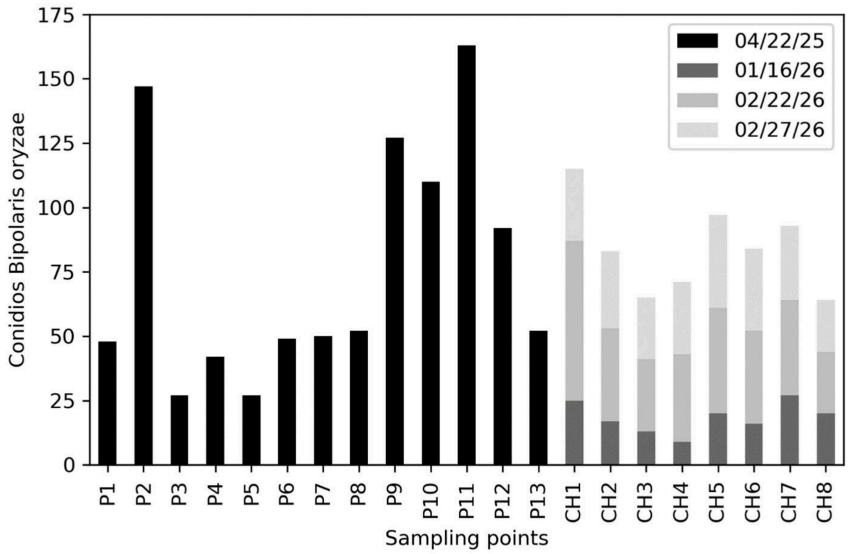

Figure 3. Number of *Bipolaris oryzae* conidia counted at each sampling point in the Paredones and Carhuaquero sectors during the monitoring dates. P and CH indicate sampling points in Paredones and Carhuaquero, respectively.

The percentage contribution of *Bipolaris oryzae* spores [26] was calculated using Equation (1). This calculation expresses the proportion of *Bipolaris oryzae* conidia relative to the total fungal spores counted on each slide. It was used as complementary evidence of the relative presence of the target pathogen around each sampling point.

$$Contribution\ (\%) = \frac{\begin{array}{c}Total\ number\ of\ colonies\ of\ a\ given\ species\\ across\ all\ observations\end{array}}{Total\ number\ of\ colonies} \times 100 \tag{1}$$

For each sampling point (marker) in the Paredones sector, three rice leaves were collected at random from each cardinal direction (E, W, N and S) at a distance of 1 m around the marker, resulting in 12 leaves per point. Leaves from each cardinal direction were stored in a coded airtight bag, and the four bags corresponding to one sampling point were placed in a larger airtight bag labeled with the sampling point code. This bag was stored in a cooler at around 4 °C using dry ice to preserve the symptomatic leaf tissue for disease severity assessment and laboratory-based pathogen identification.

Lesions present on each naturally infected leaf were analyzed for pathogen identification. Symptomatic tissues were cut into 5 mm pieces and disinfected with 1% (v/v) sodium hypochlorite, followed by consecutive washes with previously sterilized distilled water. The tissue fragments were cultured on Potato Dextrose Agar (PDA + chloramphenicol 250 mg) and incubated at 28 ± 1 °C for 7 days in the dark. Genus identification was carried out based on macro- and microscopic characteristics, using the keys of Barnett and Hunter [27].

As the disease does not occur naturally in the experimental area (Carhuaquero sector), the pathogen was artificially inoculated to ensure a consistent level of infection across treatments.

To prepare the inoculum used in the Carhuaquero sector, infected tissue pieces were placed on Petri dishes containing PDA culture medium and incubated at 28 °C in a Memmert (IN-450) incubator at 85% relative humidity for 7 to 14 days. The conidia were collected by flooding the plate surface with distilled water, scraping it with a metal spatula, and rinsing with distilled water; finally, the washings were filtered through gauze. Inoculation in the Carhuaquero plots was carried out by spraying the leaves with a hand sprayer 19 days after transplanting the seedlings. The second and third inoculations were carried out 6 and 11 weeks after transplanting, respectively.

The severity of the disease was assessed on a ten-point scale (0–9) [28], based on the proportion of leaf area affected by brown spot lesions. The score was assigned according to the estimated percentage of damaged leaf area; for example, Figure 4 shows representative leaves from Paredones, where sampling point P1S presented 1.06% affected leaf area (score 1), whereas sampling point P13S presented 7.93% affected leaf area (score 5). Figure S1 shows representative infected leaves from the Carhuaquero sector. In Carhuaquero, severity was assessed 19 days after the second inoculation and 6 and 22 days after the third inoculation.

Figure 4. Representative rice leaves showing different percentages of leaf area affected by brown spot symptoms caused by *Bipolaris oryzae*.

Disease severity scoring was performed by trained personnel from the Plant Pathology Laboratory of the Pedro Ruiz Gallo National University using the same 0–9 severity scale for all samples. To improve consistency, representative leaves were checked against the reference severity classes before assigning the final score, and the same scoring criteria were applied across sites and monitoring dates. Although no formal inter-rater reliability statistic was calculated, scoring consistency was supported by the use of a standardized scale, laboratory-based pathogen identification from symptomatic tissues, and spore monitoring at the sampling points.

2.3. Image Acquisition

Multispectral, RGB, and thermal images of the rice fields were acquired using a DJI Matrice 300 RTK UAV (DJI, Shenzhen, China). Multispectral imagery was collected with a MicaSense RedEdge camera (Micasense, Seattle, WA, USA), which captures five bands: blue, green, red, red edge, and NIR. RGB and thermal imagery were collected using the DJI Zenmuse H20T sensor (DJI, Shenzhen, China). Before each flight, the multispectral sensor was radiometrically calibrated using the manufacturer's reflectance reference panel.

The UAV operated at a flight altitude of 170 m in the Paredones sector, enabling a multispectral resolution of 12 cm pixel^{-1}. The flight time was approximately 7 min, with a speed of 7.7 m s^{-1} and frontal/lateral overlap of 80/75%. In the Carhuaquero sector, the UAV operated at a lower altitude because the experimental area was smaller, enabling a multispectral resolution of 1.4 cm pixel^{-1}. The flight time was approximately 5 min, with a speed of 1.0 m s^{-1} and frontal/lateral overlap of 85/80%. The difference in flight altitude was related to the size of the area covered at each site. A higher flight altitude was used in Paredones because the commercial field covered a larger area, whereas a lower flight altitude was feasible in Carhuaquero because the experimental area was smaller. This resulted in different spatial resolutions between sites. To reduce the influence of this difference on spectral extraction, spectral variables were calculated as mean values within standardized 1 m-radius regions of interest (ROIs) around each sampling point using radiometrically calibrated orthomosaics acquired under clear-sky conditions.

Multispectral image preprocessing included radiometric and geometric correction before spectral variable extraction. Orthomosaics were generated in Pix4D using the UAV geotagged images and the real-time kinematic (RTK) positioning and ground control point (GCP) information available for the field surveys. Geometric processing quality was evaluated using objective quality indicators, including image alignment, reprojection error, and the spatial consistency of the generated orthomosaics. No additional atmospheric correction model was applied; instead, spectral consistency relied on panel-based radiometric calibration, stable illumination conditions, and the relatively short sensor-to-target distance typical of UAV image acquisition. The calibrated orthomosaics were then used to extract mean spectral band values and vegetation indices within the 1 m-radius ROIs around each sampling point.

Vegetation indices were calculated using the equations in Table 2. Sampling points were marked using a circular ROI with a radius of one meter (Figure S2). To reduce local high-frequency noise in the UAV-derived spectral layers, a two-dimensional Savitzky–Golay smoothing filter was applied before extracting spectral values from the ROIs. Pixels corresponding to the spore-trap structure and its immediate surroundings were excluded from each ROI before calculating mean spectral values, to avoid contamination of canopy reflectance by non-vegetation elements. The vegetation indices and spectral bands for each sampling point were calculated as averages within the ROI. Figure 5 summarizes the methodological workflow used in this study.

Table 2. Vegetation indices calculated from UAV-derived multispectral bands.

Spectral Indices	Calculation Formula	Sources
Normalized Difference Vegetation Index (NDVI)	$NDVI = \frac{NIR - Red}{NIR + Red}$	[29,30]
Normalized Difference RedEdge (NDRE)	$NDRE = \frac{NIR - RedEdge}{NIR + RedEdge}$	[10,31]
Greenness Index (GI)	$GI = \frac{Green}{Blue}$	[29]
Plant Biomass Index (PBI)	$PBI = \frac{NIR}{Green}$	[32]
Ratio Vegetation Index (RVI)	$RVI = \frac{NIR}{Red}$	[10,33]

Table 2. *Cont.*

Spectral Indices	Calculation Formula	Sources
Chlorophyll Index Green (CIG)	$\text{CIG} = \frac{\text{NIR}}{\text{Green}} - 1$	[34]
Green Normalized Difference Vegetation Index (GNDVI)	$\text{GNDVI} = \frac{\text{NIR}-\text{Green}}{\text{NIR}+\text{Green}}$	[31]
Renormalized Difference Vegetation Index (RDVI)	$\text{RDVI} = \frac{\text{NIR}-\text{Red}}{\sqrt{\text{NIR}+\text{Red}}}$	[32,35]
Normalized Pigment Chlorophyll Ratio Index (NPCI)	$\text{NPCI} = \frac{\text{Red}-\text{Blue}}{\text{Red}+\text{Blue}}$	[30]

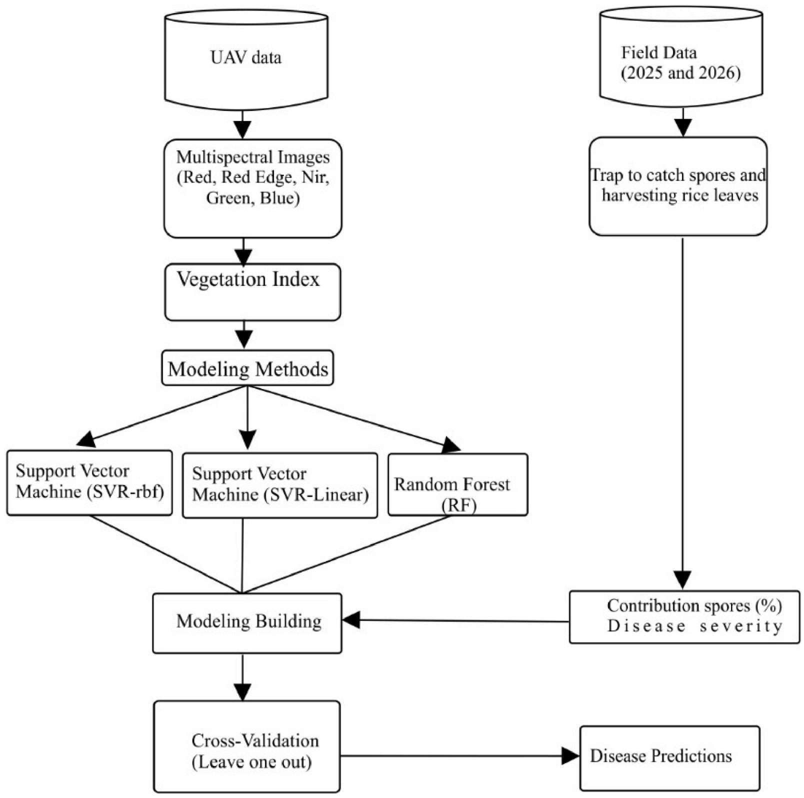

Figure 5. Flowchart for disease prediction in rice fields using machine learning models and cross-validation, employing indices and spectral bands based on UAV data.

2.4. Machine Learning Models

2.4.1. Support Vector Regression

SVMs are used for classification and regression tasks. This algorithm transforms data from a complex space into a higher-dimensional feature space [36]. This transformation enables the construction of a linear regression model in the new mapped feature space, thereby facilitating more accurate predictions [37].

Support vector regression (SVR) is based on a principle similar to that of support vector machines (SVMs), namely, finding a hyperplane that best fits a kernel-induced feature space, yielding better generalization performance than using the original features [38].

In this study, SVR models were implemented with linear and radial basis function (rbf) kernels. For both kernels, the regularization parameter was set to C = 1, epsilon was set to 0.1, and the tolerance was set to 0.001. Predictor selection was performed using Sequential Forward Selection (SFS), with leave-One-Out Cross-Validation (LOOCV-RMSE) as the optimization criterion. At each iteration, the candidate variable that produced the greatest reduction in LOOCV-RMSE was added to the model, and the subset with the lowest LOOCV-RMSE was retained. The SVR and SFS procedures were implemented in Python (Version 3) using the scikit-learn and mlxtend packages.

2.4.2. Random Forest Regression

Random Forest regression (RF), proposed by Breiman (2001) [39], is an ensemble learning technique that combines the effectiveness of decision trees with randomness. It constructs a large number of decision trees using random subsets of the training data and randomly selected subsets of the input variables. Each decision tree makes independent predictions, and the final prediction is obtained by averaging across all trees [40]. Its effectiveness lies in its robustness to high-dimensional data and outliers [41]. Due to its robustness, it is used for classification and regression [11]. In agricultural applications, the RF model demonstrated greater accuracy in identifying areas affected by rice false smut, a fungal disease of rice panicles caused by the ascomycete fungus *Ustilaginoidea virens* [42]. In predicting the severity of late blight in potato crops, using multispectral images obtained by UAV, RF showed remarkably good performance [43].

In this study, the RF model was implemented in Python using the scikit-learn package. Hyperparameter tuning was performed using grid search, with LOOCV-RMSE as the optimization criterion. The evaluated hyperparameters were the number of trees, maximum tree depth, and the number of predictors considered at each split. The number of trees was evaluated from 1 to 180, the maximum tree depth from 3 to 20, and max_features from 2 to 16.

2.5. Feature Selection and Multicollinearity Assessment

Feature selection was performed using SFS. The procedure started with an empty predictor set and iteratively added the candidate variable that produced the largest reduction in LOOCV-RMSE. At each iteration, model performance was evaluated using RMSE as the selection criterion. The process continued until all candidate variables had been evaluated, and the subset with the lowest LOOCV-RMSE was retained as the optimal feature combination. To assess multicollinearity among candidate predictors, the variance inflation factor (VIF) was calculated before model fitting.

2.6. Validation Methods

To evaluate model performance in estimating rice brown spot severity at the canopy level, the coefficient of determination (R^2), root mean square error (RMSE), and relative root mean square error (rRMSE) were calculated. Model performance was assessed using LOOCV [31], in which each observation was used once as the validation sample and the remaining observations were used for training. To reduce the risk of data leakage, SFS-based feature selection was performed within the LOOCV procedure. In each iteration, feature selection and model fitting were performed using only the training observations, and the fitted model was then used to predict the held-out observation.

$$R^2 = 1 - \frac{\sum_{j=1}^{n} \left(Y_j - \hat{Y}_j\right)^2}{\sum_{j=1}^{n} \left(Y_j - \hat{Y}\right)^2} \tag{2}$$

$$RMSE = \sqrt{\frac{\sum_{j=1}^{n} \left(Y_j - \hat{Y}_j\right)^2}{n}} \tag{3}$$

$$rRMSE = \frac{RMSE}{\overline{Y}} \times 100 \tag{4}$$

where n is the total number of sampling points; Y_i and $\hat{Y}_j$ denote the jth measured and predicted values of rice disease, respectively; $\overline{Y}$ is the average of the severity levels.

3. Results

3.1. Correlation Coefficient

Table 3 presents the Pearson correlation analysis between the severity of rice brown spot caused by *Bipolaris oryzae* and various vegetation indices and spectral bands for the phenological stages of the vegetative, flowering, and milk-ripening stages. Pearson correlation was used as an exploratory measure of linear association because the 0–9 severity score was treated as an ordered numerical response in the regression analysis. The correlations were calculated using the complete dataset of 37 sampling observations from both study sites and all evaluated growth stages. This pooled analysis was used to describe the overall association between UAV-derived spectral variables and field-assessed rice brown spot severity, because the number of observations within each site or growth stage was limited. Statistical significance was interpreted using $p < 0.05$ as the general threshold, and additional significance levels were indicated in Table 3 for clarity (ns, $p \geq 0.05$; *, $p < 0.05$; **, $p < 0.01$; ***, $p < 0.001$). Table 3 shows that a group of indices exhibited strong and highly significant negative correlations ($p < 0.001$) with the severity level, in particular the NDRE (r = −0.83), GNDVI (r = −0.82), NDVI (r = −0.80), PBI (r = −0.74), CIG (r = −0.74), RVI (r = −0.73), RDVI (r = −0.67), GI (r = −0.57) and NIR (r = −0.52). In contrast, the NPCI (r = 0.77, $p < 0.001$) and the RED spectral band (r = 0.60, $p < 0.001$) showed positive and highly significant correlations with severity. Meanwhile, the GREEN spectral band (r = 0.37, $p < 0.05$) and the percentage incidence of spores (CON, r = 0.40, $p < 0.05$) showed positive correlations with severity. However, the RED EDGE (r = 0.30, ns) and BLUE (r = 0.18, ns) spectral bands showed a very weak positive correlation with severity levels.

Table 3. Pearson correlation coefficients between spectral variables, conidial counts, and rice brown spot severity during 2025–2026.

Spectral Variable	Correlation Coefficient (r)	*p*-Value
NDRE	−0.83 ***	0.0000
GNDVI	−0.82 ***	0.0000
NDVI	−0.80 ***	0.0000
CIG	−0.74 ***	0.0000
PBI	−0.74 ***	0.0000
RVI	−0.73 ***	0.0000
RDVI	−0.67 ***	0.0000
GI	−0.57 ***	0.0002
NIR	−0.52 ***	0.0009
NPCI	0.77 ***	0.0000
RED	0.60 ***	0.0001
GREEN	0.37 *	0.0256
CON	0.40 *	0.0140
RED EDGE	0.30 ns	0.0758
BLUE	0.18 ns	0.2848

Note: ns is not significant at the $p \geq 0.05$ level; * is significantly correlated at the $p < 0.05$ level; and *** is significantly correlated at the $p < 0.001$ level.

3.2. Rice Disease Prediction Models Using Support Vector Regression (SVR)

Predictive models for rice brown spot severity were developed using SVR. To construct the models, SVR was combined with SFS, which starts with an empty predictor set and iteratively adds the variable that most improves model performance. The reported cross-validated performance was obtained using the LOOCV procedure described in Section 2.6, in which feature selection was performed within each training fold to reduce the risk of data leakage.

Figure 6 shows the SFS process used to identify the predictor subsets for the SVR-rbf and SVR-linear models. The procedure started with an empty predictor set and added one variable at each iteration according to the reduction in LOOCV-RMSE. Therefore, the *x*-axis represents the number of variables included in the model, whereas the *y*-axis represents the corresponding cross-validated RMSE. The selected subset was the one with the lowest LOOCV-RMSE. For SVR-rbf, the lowest error was obtained using NDRE alone, whereas for SVR-linear, the lowest error was obtained using NDRE, GREEN, and BLUE. These results indicate that adding more variables did not further improve the cross-validated prediction error under the available dataset. Thus, the selected subsets were retained because they achieved the minimum LOOCV-RMSE among the evaluated SFS candidate subsets, rather than because of their individual correlations alone.

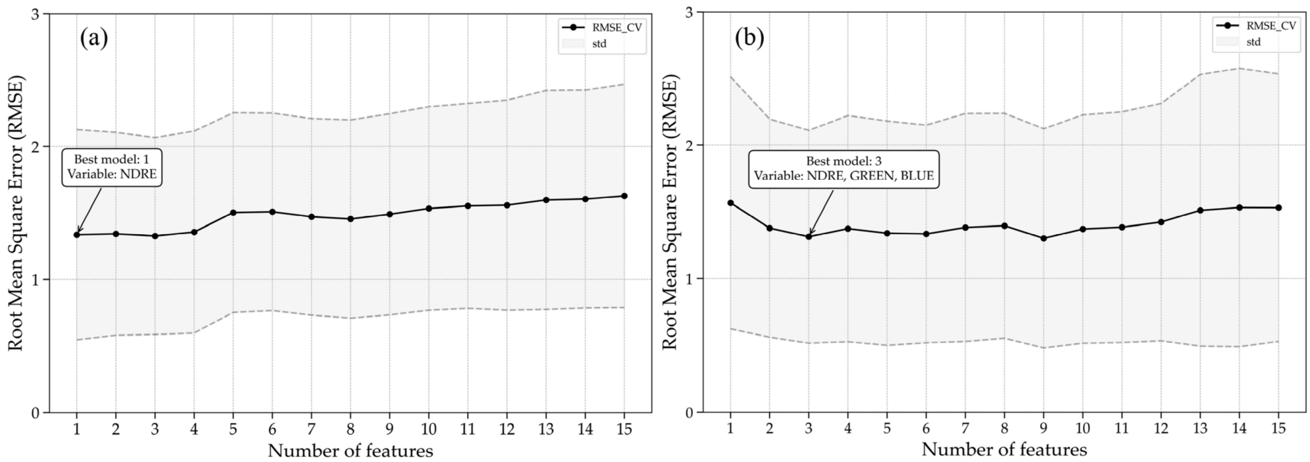

Figure 6. Evolution of the root mean square error (RMSE) as a function of the number of features selected using SFS for (**a**) SVR-rbf and (**b**) SVR-linear during the vegetative, flowering and milk-ripening stages. The selected predictor subset in each case is indicated, together with the corresponding selected variables.

The multicollinearity assessment showed redundancy among several vegetation indices, particularly between NDRE and NDVI. However, the SFS procedure did not retain both variables in the selected SVR predictor subsets. This indicates that NDRE provided sufficient predictive information without the simultaneous inclusion of NDVI, reducing redundant spectral information while preserving the physiological relevance of the selected predictors.

The scatter plots in Figure 7 illustrate the relationships between observed and predicted severity levels for the SVR-rbf and SVR-linear models, selected using SFS. During the vegetative, flowering, and milk-ripening stages of rice, the SVR-rbf model incorporated the NDRE variable, achieving R^2_CV = 0.75, RMSE_CV = 1.34, and rRMSE_CV = 35.45%. Under the same conditions, the SVR-linear model selected the variables NDRE, GREEN, and BLUE, achieving an R^2_CV = 0.76, an RMSE_CV = 1.31, and an rRMSE_CV = 34.85%. Although the BLUE band showed a weak and non-significant individual correlation with disease severity (r = 0.18; Table 3), it was retained in the optimal SVR-linear model after NDRE and GREEN were included. This result indicates that BLUE did not act as an independent univariate predictor, but provided complementary information in the multivariate feature space. In SFS, variables are selected according to their contribution to reducing the LOOCV-RMSE of the complete model rather than according to their individual Pearson correlation with the response variable. Therefore, the inclusion of BLUE suggests that this band contributed to improving prediction when combined with NDRE and GREEN, possibly by capturing residual spectral variability not represented by the red-edge and green-related predictors. However, this result should be interpreted as model-dependent and not as evidence that BLUE alone is a strong disease-severity indicator. In both models, the points lie close to the 1:1 reference line, indicating a relationship between the observed and predicted severity levels. Although the SVR-linear model showed the lowest RMSE_CV, the differences among SVR-linear, SVR-rbf, and RF were small. Therefore, the results should not be interpreted as evidence of clear superiority of one algorithm, but rather as an indication that the evaluated models achieved comparable predictive performance under the available dataset. These results indicate that UAV-derived spectral variables provided useful but moderate predictive information for estimating field-assessed rice brown spot severity under the evaluated conditions. However, because the models were developed from a limited dataset, their performance should be interpreted as preliminary and requires validation with larger independent datasets.

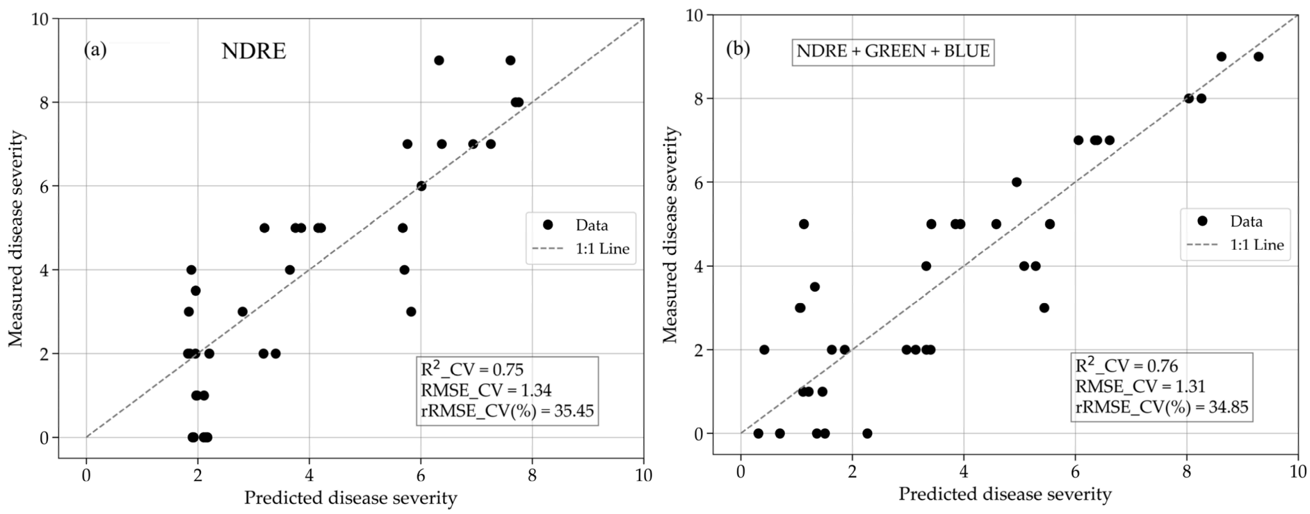

Figure 7. Relationship between observed and predicted rice brown spot severity levels caused by *Bipolaris oryzae* for the best-performing models, selected using SFS: (**a**) SVR-rbf and (**b**) SVR-linear, both at the vegetative, flowering and milk-ripening stages.

3.3. Random Forest Model for Predicting Rice Disease

An RF model was constructed to predict rice brown spot severity during the vegetative, flowering and milk-ripening stages in 2025 and 2026. The analysis was based on a total of $n = 37$ sampling points.

The RF model was tuned by evaluating the number of trees and the subset of spectral predictors. Figure 8a shows the out-of-bag (OOB) error as the number of trees increased; the error stabilized after the initial trees, and the best configuration was obtained with 161 trees. Figure 8b shows the feature-selection process based on LOOCV-RMSE, where predictor subsets were evaluated according to their contribution to reducing cross-validated error. The RF predictor subset was selected at the point where LOOCV-RMSE reached its minimum, indicating that larger subsets did not provide a clear additional reduction in prediction error. Figure 8c shows the relative importance of the predictors in the final RF model, expressed as percentage increase in mean squared error (%IncMSE). Higher

%IncMSE values indicate that permuting that predictor caused a larger decrease in model performance, suggesting a greater contribution to the RF prediction.

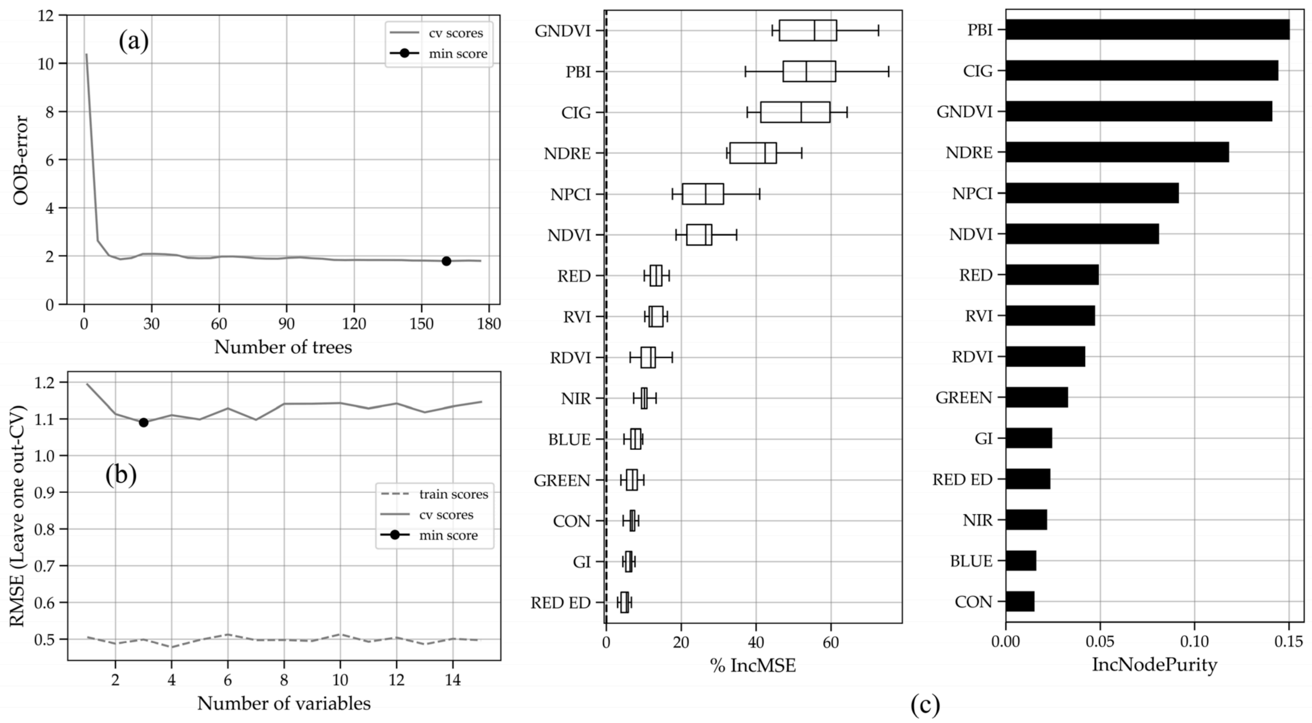

Figure 8. RF model for predicting rice brown spot severity during the vegetative, flowering and milk-ripening stages (2025–2026) using vegetation indices and spectral bands: (**a**) out-of-bag error (OOB), (**b**) feature selection using Leave-One-Out cross-validation (RMSE) and (**c**) predictor importance.

Figure 9 shows the predicted disease severity levels in rice fields compared with the measured severity levels.

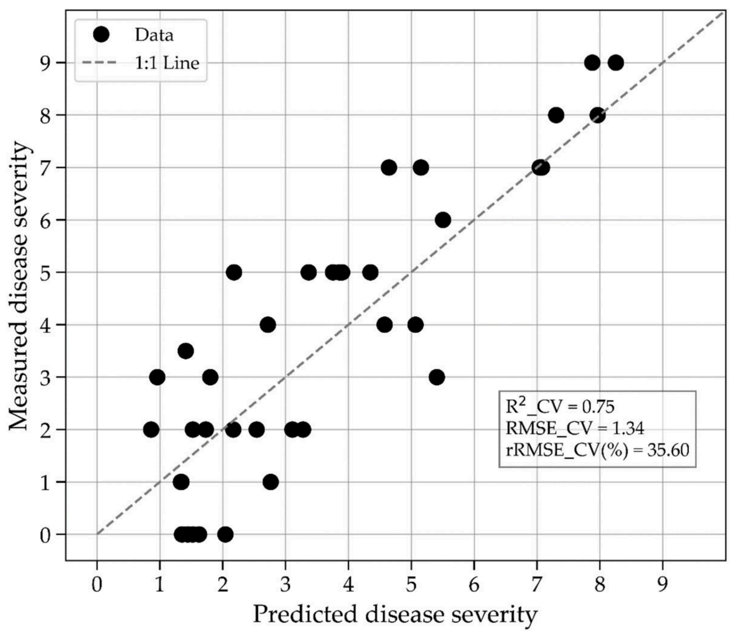

Figure 9. Predicted versus observed disease severity levels in rice fields for the RF model, using vegetation indices and spectral bands during the vegetative, flowering and milk-ripening stages in 2025–2026.

At the vegetative, flowering, and milk-ripening stages, the RF model based on indices and spectral bands achieved moderate predictive performance, with a coefficient of determination (R^2_CV) of 0.75, an RMSE_CV of 1.34, and an rRMSE (%) of 35.60%.

Table 4 summarizes the performance of the disease prediction models using two machine-learning approaches: SVR and RF. The models obtained were validated using LOOCV. For the RF model, the OOB error was used to evaluate the number of trees, whereas LOOCV-RMSE was used for predictor subset selection and model comparison.

Table 4. Performance of the machine learning models for predicting rice brown spot severity during the vegetative, flowering, and milk-ripening stages for 2025–2026, using leave-one-out cross-validation.

Machine Learning Models	Leave–One-Out Cross Validation (LOOCV)		
	R^2_CV	RMSE	rRMSE (%)
Support Vector Regression (SVR-rbf)	0.75	1.34	35.45
Support Vector Regression (SVR-linear)	0.76	1.31	34.85
Random Forest (RF)	0.75	1.34	35.60

According to Table 4, the three models showed comparable predictive performance. The SVR-linear model presented the slightly lowest RMSE_CV (1.31) and highest R^2_CV (0.76), whereas SVR-rbf and RF showed very similar results (R^2_CV = 0.75; RMSE_CV = 1.34). However, the rRMSE values were close to 35% in all models, indicating moderate prediction error. Therefore, the small differences among models should be interpreted cautiously, and the results should be considered as preliminary evidence of the potential of UAV-derived multispectral variables for brown spot severity estimation rather than as evidence of strong prediction ability.

4. Discussion

4.1. Relationship Between Vegetation Indices and Disease Severity

UAV-based remote sensing has been increasingly used for rice disease monitoring [8,10,32], and the results of this study suggest that UAV-derived multispectral variables can also provide useful information for estimating rice brown spot severity under field conditions.

Rice brown spot disease, caused by *Bipolaris oryzae*, induces a series of changes in physiological and biochemical parameters [16]. In the present study, rice plants inoculated with the fungus *Bipolaris oryzae* experienced biotic stress, which may affect normal development and contribute to reductions in green leaf area and biomass. These responses are consistent with Almeida et al. [16], who reported reductions in photosynthetic pigments and alterations in physiological performance in rice plants exposed to drought stress and *Bipolaris oryzae* infection. From a remote-sensing perspective, such physiological changes can modify canopy reflectance mainly in the visible, red-edge, and NIR regions because plant diseases and stress alter pigment concentration, photosynthetic activity, and leaf/canopy structure [44]. Chlorophyll loss associated with disease stress can reduce light absorption in the red region, which may increase red reflectance, whereas necrotic lesions, changes in leaf internal structure, and reductions in green leaf area can affect NIR reflectance [17,45]. The red-edge region is particularly sensitive to canopy chlorophyll-related properties, and red-edge-based indices have shown strong performance for estimating crop chlorophyll and nitrogen content [46]. In addition, changes in plant pigments can be sensitively detected using UAV-based hyperspectral data, as reported by Feng et al. [35].

Therefore, the negative correlations observed for NDRE, NDVI, GNDVI, RVI, and NIR, and the positive correlations observed for NPCI and RED, are biologically consistent with disease-induced pigment degradation, photosynthetic impairment, and structural damage in infected rice plants. Although these spectral responses are biologically consistent with brown spot-induced damage, they should be interpreted together with field severity assessments, spore monitoring, and pathogen identification, because similar changes in pigment concentration, canopy vigor, biomass, and leaf/canopy structure may also occur under other stress conditions.

The NDRE index showed the strongest negative correlation with disease severity (r = −0.83; Table 3). This response is mechanistically plausible because the red-edge region is highly sensitive to variations in chlorophyll content and canopy vigor. As brown spot severity increases, chlorophyll degradation and lesion expansion reduce the spectral contrast captured by NDRE, leading to lower NDRE values in more severely affected plants [47].

High NDVI values were associated with low levels of brown spot disease severity, resulting in a negative correlation of −0.80 (Table 3). Zhang et al. [48] reported a similar result when they analyzed the relationship between disease severity and NDVI, enabling quantification of disease severity levels in rice field plots.

Healthy vegetation reflects more NIR radiation and absorbs more red light, resulting in high RVI reflectance ratios (RVI = NIR/RED) [49,50]. Another index that correlated negatively with disease severity is the RVI (r = −0.73). This is because brown spot disease alters the pigmentation and structure of leaves, thereby changing the reflectance properties of infected plants. Consequently, diseased plants may exhibit lower RVI values than healthy plants [49,50].

Meanwhile, the NPCI (r = 0.77) showed a positive correlation with disease severity. According to Peñuelas et al. [51], the NPCI acts as a rough estimate of the ratio between total pigments and chlorophyll a, and the NPCI decreases in healthy plants and increases in stressed plants, as observed in this study. The NPCI proved suitable for assessing different levels of infection in wheat; however, the index's performance varies considerably across different growth stages [48].

The RED spectral band showed a positive correlation with disease levels (Table 3), whilst the NIR spectral band showed a negative correlation. In previous studies [8], it was observed that as the degree of infection by *Pyricularia* increased, reflectance values in the RED spectral band increased. Although spectral bands exhibit variable responses to the physiological and biochemical properties of plants, the values in the RED and RED EDGE regions proved to be the most sensitive to diseases such as *Pyricularia*, tungro, and bacterial blight of rice, caused by viruses, bacteria, and fungi [52].

4.2. Performance of Machine Learning Models

The results of this study indicate that UAV-derived spectral bands and vegetation indices can provide useful information for estimating the severity of rice brown spot caused by *Bipolaris oryzae* during the vegetative, flowering, and milk-ripening stages. The support vector regression model with a linear kernel (SVR-linear), validated using LOOCV, showed the slightly lowest prediction error (R^2_CV = 0.76), followed by the SVR-rbf model (R^2_CV = 0.75). The absence of NDVI from the best-performing SVR models may be explained by its redundancy with NDRE. Although both indices were strongly correlated with disease severity, NDRE showed the strongest association and provides red-edge information that is more directly related to chlorophyll-sensitive canopy responses. Therefore, the SFS procedure favored NDRE over NDVI, reducing redundant spectral information while preserving the physiological relevance of the selected predictors.

Saeed et al. [53] demonstrated that SVM-rbf was the best algorithm for predicting the geographical origin of white rice among the various algorithms tested, achieving an accuracy of 0.99 in LOOCV. A key advantage of SVM is its ability to generalize from small datasets [54]. However, Zhao et al. [8] reported that the SVM algorithm did not yield the best results for detecting Pyricularia disease in rice. Furthermore, the RF model reached an R^2_CV of 0.75 (Table 4), with an RMSE of 1.34, slightly higher than that of the SVR-linear model, indicating comparable performance. Tripathi et al. [55] found that among all models, the RF model achieved the highest accuracy in predicting rice yield, with an RMSE of 0.27 t ha^{-1}. Similar findings were reported by Quille-Mamani et al. [31], who integrated vegetation and texture indices to forecast rice yield at different phenological stages. The integration of spectral and textural features derived from UAV multispectral imagery has been reported to improve rice disease detection [11]; therefore, future studies should evaluate whether textural features can improve brown spot severity estimation.

Previous remote-sensing studies on rice brown spot have mainly relied on hyperspectral reflectance measured at the leaf or canopy scale. Liu et al. [17] reported high prediction accuracy for brown spot severity using leaf-level hyperspectral data, with validation RMSE values as low as 2.0% for partial least-squares regression and 5.8% for stepwise regression. Similarly, Liu et al. [45] characterized brown spot severity using laboratory and field hyperspectral reflectance data, confirming the sensitivity of spectral information to disease-induced canopy changes. Compared with these studies, the present work achieved moderate predictive performance at the field scale (SVR-linear: R^2_CV = 0.76; RMSE_CV = 1.31) using bands extracted from UAV-acquired multispectral imagery and vegetation indices under field conditions. This difference is expected because hyperspectral measurements provide many narrow bands and are often acquired under more controlled conditions, whereas UAV multispectral imagery uses fewer broad bands and is more affected by field heterogeneity, canopy structure, illumination, spatial resolution, and geolocation uncertainty. Therefore, the main advantage of this study is not higher accuracy than leaf-level hyperspectral approaches, but its field-scale applicability using UAV multispectral imagery and a reduced set of predictors.

Classification results from previous studies should not be directly compared with the regression metrics reported in this study. Many rice disease studies report accuracy, precision, recall, or F1-score because they classify healthy and diseased plants or disease categories. In contrast, this study estimated brown spot severity on a 0–9 scale using regression models and evaluated performance using R^2_CV, RMSE_CV, and rRMSE_CV. Therefore, classification studies were used only as methodological context, not as direct benchmarks for model performance.

Comparisons with previous studies should be interpreted cautiously because several cited works differ from the present study in target disease, sensor type, crop, spatial scale, or prediction objective. Studies on rice blast, false smut, other crop diseases, hyperspectral data, or satellite imagery provide useful methodological context, but their accuracy metrics are not directly comparable with those obtained here for UAV-based estimation of rice brown spot severity. Therefore, these studies were used mainly to support the broader remote-sensing and machine-learning framework for crop disease assessment, whereas the specific contribution of this work is the field-scale estimation of *Bipolaris oryzae* severity in rice using UAV-derived multispectral variables under Peruvian conditions.

4.3. Study Limitations and Future Research

Despite the promising associations observed between UAV-derived spectral variables and field-assessed brown spot severity, the results should be interpreted cautiously. The predictive performance obtained in this study reflects the combined influence of disease symptoms, canopy condition, phenological stage, site-specific management, image resolution, and field-assessment uncertainty. Therefore, the models should not be interpreted as fully transferable diagnostic tools, but as preliminary field-scale models developed under the specific conditions evaluated in this study.

One important limitation is that the dataset combined observations from different phenological stages, including vegetative, flowering, and milk-ripening stages. This may have affected model robustness because the spectral characteristics of cereal crops change dynamically during growth [51].

Model uncertainty may also be associated with differences in disease occurrence conditions between the two study areas and with the interaction between host resistance and crop management. The experiment was conducted on the *El Valor* variety, which is resistant to pests and fungal diseases. This resistance may have limited symptom development and reduced the spectral contrast between healthy and infected plants, particularly under low disease pressure. In Paredones, brown spot occurred under natural infection conditions in a commercial rice field, where fungicide applications were used as part of standard crop management to control the disease and prevent yield decline. Consequently, no symptoms were observed at six sampling points, whereas mild infection was observed at seven points. In contrast, the Carhuaquero experiment involved artificial inoculation under a more controlled field setting and showed a wider severity range, from 2 to 9. Despite differences in infection conditions between sites, symptom expression was consistent with the characteristic brown spot symptoms associated with *Bipolaris oryzae*, and pathogen presence was supported by spore monitoring and laboratory identification. Therefore, disease severity assessments from both sites were considered to reflect the same host–pathogen interaction and were used jointly for model development. The datasets from both sites were combined to increase the range of field-assessed brown spot severity available for model development, rather than to compare natural infection and artificial inoculation as separate treatments. However, these contrasting disease conditions may have increased the heterogeneity of the spectral–severity relationships used for model training. In addition, the UAV flight altitude differed between sites because the area covered in Paredones was substantially larger than that in Carhuaquero, resulting in different spatial resolutions that may have affected the spectral information extracted within the 1 m-radius ROIs.

Field survey uncertainty should also be considered because disease severity was visually assessed on leaves and may be affected by observer judgment, lesion distribution within the canopy, and the representativeness of the sampled leaves around each post.

The rRMSE values of approximately 35% indicate moderate prediction error, which limits the strength of the conclusions that can be drawn from the models. The limited number of sampling observations (n = 37) is another important constraint, because small datasets can increase model instability and limit the generalizability of machine-learning results. Although LOOCV was used to maximize the use of the available data and provide an internal estimate of predictive performance, it does not replace validation with independent field data. Therefore, although the proposed models show potential for estimating brown spot severity under field conditions, their predictive capacity should be interpreted as preliminary. This limitation should be interpreted in light of the limited sample size, site heterogeneity, differences in spatial resolution, and possible field-assessment uncertainty.

Therefore, the current models should not be considered ready for operational disease management or direct decision-making in precision agriculture. Their use should remain limited to exploratory plot-level severity estimation until they are validated with larger, independent, and more representative datasets. Future research should include larger datasets, more balanced severity levels, standardized flight heights, independent validation fields, repeated severity assessments, and complementary predictors such as textural and thermal features to improve model robustness and transferability.

https://doi.org/10.3390/drones10070495

Another source of uncertainty is that the spectral indices used in this study are sensitive to general crop stress rather than exclusively to brown spot infection. Therefore, the disease effect could not be fully isolated from crop stage, site-specific conditions, water or nutrient status, and fungicide effects under the field-based design used in this study. Instead, the interpretation of the spectral response as related to brown spot severity was supported by three lines of evidence: field-based severity scoring using a standardized 0–9 scale, spore monitoring at the sampling points, and laboratory-based identification of *Bipolaris oryzae* from symptomatic tissues. In addition, all observations corresponded to the same rice variety, which reduced varietal variability. However, vegetation indices based on visible, red-edge, and NIR reflectance are commonly associated with changes in chlorophyll content, canopy vigor, biomass, and structural properties, which may also be affected by phenological stage, water or nutrient status, and crop management practices [44,56]. Although disease severity was assessed in the field and symptomatic tissues were used for pathogen identification, spectral responses may also have been influenced by these non-disease factors. Therefore, the models should be interpreted as tools for estimating field-assessed brown spot severity under the evaluated conditions, rather than as disease-specific diagnostic models able to isolate *Bipolaris oryzae* effects from all other stress factors. Future studies should include controlled treatments, independent validation fields, and complementary variables such as soil moisture, nutrient status, thermal information, and management records to better separate disease effects from other sources of crop stress.

5. Conclusions

- In this study, UAV multispectral imagery was used to estimate the field-scale severity of rice brown spot caused by *Bipolaris oryzae*. Several vegetation indices and spectral bands were evaluated as predictors across the vegetative, flowering, and milk-ripening stages.
- Among the evaluated models, SVR-linear showed the slightly lowest prediction error with NDRE, GREEN, and BLUE selected as the most relevant predictors. However, the performance of SVR-linear, SVR-rbf, and RF was very similar, and the rRMSE values of approximately 35% indicate moderate prediction error. Therefore, the results should be interpreted as preliminary evidence that UAV-derived multispectral information can support plot-level estimation of rice brown spot severity, rather than as evidence of strong predictive accuracy.
- The models were evaluated using LOOCV, which was appropriate for maximizing the use of the available data given the limited number of sampling observations. However, because the dataset comprised only 37 sampling observations and no independent external validation was performed, the reported performance should be interpreted as preliminary and should not be considered evidence of full model robustness or broad transferability.
- These findings directly address the limitations of conventional disease monitoring, which is labor-intensive, time-consuming, and spatially discontinuous. In practical terms, spatial outputs derived from this type of model could support targeted field scouting and, after further validation, precision-management actions such as prioritizing areas for phytosanitary intervention or guiding variable-rate fungicide application.
- The main limitations of this study include the limited sample size, the combination of different growth stages, contrasting field conditions between sites, different disease establishment conditions, and unbalanced disease severity levels. Therefore, practical implementation requires further research with larger datasets, independent validation fields, and more balanced disease severity gradients to improve model robustness, transferability, and operational applicability.

Supplementary Materials: The following supporting information can be downloaded at: https://www.mdpi.com/article/10.3390/drones10070495/s1. Figure S1: infected leaves from the Carhuaquero sector; Figure S2: workflow for extracting mean spectral variables in the vicinity of each post; Figure S3: representative images of fieldwork showing the installed posts, spore traps, the leaf sampling area, and the UAV flight configuration.

Author Contributions: Conceptualization, J.A.-L. and L.R.-F.; methodology, J.A.-L. and M.J.-C.; validation, J.A.-L. and J.V.; formal analysis, J.A.-L.; investigation, J.V. and J.A.-L.; resources, L.R.-F.; data curation, J.V.; writing—original draft preparation, J.A.-L.; writing—review and editing, M.J.-C., J.V., L.Á.R. and L.R.-F.; visualization, J.A.-L.; supervision, L.R.-F.; project administration, L.R.-F.; funding acquisition, L.R.-F. and J.A.-L. All authors have read and agreed to the published version of the manuscript.

Funding: This work was funded by PROCIENCIA-Peru, through the project: "Early warning system for detecting the emergence of pests and diseases using artificial intelligence and remote sensing in rice fields in the Lambayeque Region", under contract N°. PE501090091-2024-PROCIENCIA.

Data Availability Statement: The data presented in this study are available upon request from the corresponding author.

Acknowledgments: The authors would also like to thank the anonymous reviewers for their valuable contributions, which helped to improve this article.

Conflicts of Interest: The authors declare no conflicts of interest.

References

1. Bautista, A.S.; Tarrazó-Serrano, D.; Uris, A.; Blesa, M.; Estruch-Guitart, V.; Castiñeira-Ibáñez, S.; Rubio, C. Remote Sensing Evaluation Drone Herbicide Application Effectiveness for Controlling *Echinochloa* spp. in Rice Crop in Valencia (Spain). *Sensors* **2024**, *24*, 804. [CrossRef]
2. Chakraborty, B.; Banerjee, S.; Samanta, S.; Debangshi, U.; Yadav, S.V.; Khaire, P.B.; Shelar, V.B.; Bansode, G.D.; Landage, K.B. Detection of Rice Blast Disease (Magnaporthe Grisea) Using Different Machine Learning Techniques. *Int. J. Environ. Clim. Change* **2023**, *13*, 2256–2264. [CrossRef]
3. Zheng, Q.; Huang, W.; Xia, Q.; Dong, Y.; Ye, H.; Jiang, H.; Chen, S.; Huang, S. Remote Sensing Monitoring of Rice Diseases and Pests from Different Data Sources: A Review. *Agronomy* **2023**, *13*, 1851. [CrossRef]
4. Sahasranamam, V.; Ramesh, T.; Rajeswari, R. Monitoring and Identifying Paddy Leaf Diseases Using Unmanned Aerial Vehicles (UAVs) with Machine Learning—A Survey. In *Proceedings of the 2023 IEEE 2nd International Conference on Industrial Electronics: Developments and Applications, ICIDeA, Imphal, India, 29–30 September 2023*; Institute of Electrical and Electronics Engineers Inc.: New York, NY, USA; pp. 560–566. [CrossRef]
5. Zualkernan, I.; Abuhani, D.A.; Hussain, M.H.; Khan, J.; ElMohandes, M. Machine Learning for Precision Agriculture Using Imagery from Unmanned Aerial Vehicles (UAVs): A Survey. *Drones* **2023**, *7*, 382. [CrossRef]
6. Liu, T.; Qi, Y.; Yang, F.; Yi, X.; Guo, S.; Wu, P.; Yuan, Q.; Xu, T. Early Detection of Rice Blast Using UAV Hyperspectral Imagery and Multi-Scale Integrator Selection Attention Transformer Network (MS-STNet). *Comput. Electron. Agric.* **2025**, *231*, 110007. [CrossRef]
7. Gu, C.; Cheng, T.; Cai, N.; Li, W.; Zhang, G.; Zhou, X.G.; Zhang, D. Assessing Narrow Brown Leaf Spot Severity and Fungicide Efficacy in Rice Using Low Altitude UAV Imaging. *Ecol. Inform.* **2023**, *77*, 102208. [CrossRef]
8. Zhao, D.; Cao, Y.; Li, J.; Cao, Q.; Li, J.; Guo, F.; Feng, S.; Xu, T. Early Detection of Rice Leaf Blast Disease Using Unmanned Aerial Vehicle Remote Sensing: A Novel Approach Integrating a New Spectral Vegetation Index and Machine Learning. *Agronomy* **2024**, *14*, 602. [CrossRef]
9. Tian, L.; Wang, Z.; Xue, B.; Li, D.; Zheng, H.; Yao, X.; Zhu, Y.; Cao, W.; Cheng, T. A Disease-Specific Spectral Index Tracks Magnaporthe Oryzae Infection in Paddy Rice from Ground to Space. *Remote Sens. Environ.* **2023**, *285*, 113384. [CrossRef]
10. Agenjos-Moreno, A.; Rubio, C.; Uris, A.; Simeón, R.; Franch, B.; Domingo, C.; Bautista, A.S. Strategy for Monitoring the Blast Incidence in Crops of Bomba Rice Variety Using Remote Sensing Data. *Agriculture* **2024**, *14*, 1385. [CrossRef]
11. Su, H.; Pan, Y.; Qin, L.; Wu, G.; Shi, C.; Wang, Y.K.; Hua, S.; Luo, S.W. Research on the Monitoring Method of Rice Blast Disease at Canopy Scale Based on UAV Multispectral Imaging. In Proceedings of the Chinese Control Conference, CCC, Kunming, China, 28–31 July 2024. [CrossRef]
12. Das, S.; Biswas, A.; Vimalkumar, C.; Sinha, P. Deep Learning Analysis of Rice Blast Disease Using Remote Sensing Images. *IEEE Geosci. Remote Sens. Lett.* **2023**, *20*, 2500905. [CrossRef]

13. Wijayanto, A.K.; Prasetyo, L.B.; Hudjimartsu, S.A.; Sigit, G.; Hongo, C. Textural Features for BLB Disease Damage Assessment in Paddy Fields Using Drone Data and Machine Learning: Enhancing Disease Detection Accuracy. *Smart Agric. Technol.* **2024**, *8*, 100498. [CrossRef]
14. Ashfaq, B.; Arshad, H.M.I.; Atiq, M.; Yousaf, S.; Saleem, K.; Arshad, A. Biochemical Profiling of Resistant Phenotypes Against *Bipolaris oryzae* Causing Brown Spot Disease in Rice. *Front. Agron.* **2021**, *3*, 675895. [CrossRef]
15. Kaboré, K.H.; Kassankogno, A.I.; Tharreau, D. Brown Spot of Rice: Worldwide Disease Impact, Phenotypic and Genetic Diversity of the Causal Pathogen Bipolaris Oryzae, and Management of the Disease. In *Plant Pathology*; John Wiley and Sons Inc.: Hoboken, NJ, USA, 2025; pp. 908–922. [CrossRef]
16. Almeida, L.C.; do Nascimento, L.T.D.; Santiago, T.R.; dos Santos, M.A.; de Souza, E.R.; Rios, J.A. Biochemical and Physiological Responses of Rice Plants to the Combined Occurrence of Drought Stress and Infection by Bipolaris Oryzae. *Eur. J. Plant Pathol.* **2026**, *174*, 989–1003. [CrossRef]
17. Liu, Z.-Y.; Huang, J.-F.; Shi, J.-J.; Tao, R.-X.; Zhou, W.; Zhang, L.-L. Characterizing and Estimating Rice Brown Spot Disease Severity Using Stepwise Regression, Principal Component Regression and Partial Least-Square Regression. *J. Zhejiang Univ. Sci. B* **2007**, *8*, 738–744. [CrossRef] [PubMed]
18. Zhao, J.; Zhang, D.; Luo, J.; Dong, Y.; Yang, H.; Huang, W. Characterization of the Rice Canopy Infested with Brown Spot Disease Using Field Hyperspectral Data. *Wuhan Univ. J. Nat. Sci.* **2012**, *17*, 86–92. [CrossRef]
19. Seelwal, P.; Dhiman, P.; Gulzar, Y.; Kaur, A.; Wadhwa, S.; Onn, C.W. A Systematic Review of Deep Learning Applications for Rice Disease Diagnosis: Current Trends and Future Directions. *Front. Comput. Sci.* **2024**, *6*, 1452961. [CrossRef]
20. Sahoo, S.; Singha, C.; Govind, A.; Sharma, M. Leveraging ML to Predict Climate Change Impact on Rice Crop Disease in Eastern India. *Environ. Monit. Assess.* **2025**, *197*, 366. [CrossRef] [PubMed]
21. Upadhyay, S.K.; Kumar, A. A Novel Approach for Rice Plant Diseases Classification with Deep Convolutional Neural Network. *Int. J. Inf. Technol.* **2022**, *14*, 185–199. [CrossRef]
22. Li, L.; Zhao, H.; Liu, N. MCD-Yolov5: Accurate, Real-Time Crop Disease and Pest Identification Approach Using UAVs. *Electronics* **2023**, *12*, 4365. [CrossRef]
23. Martins, O.O.; Oosthuizen, C.C.; Desai, D.A. RiceLeafClassifier-v1.0: A Quantized Deep Learning Model for Automated Rice Leaf Disease Detection and Edge Deployment. *Eng. Rep.* **2025**, *7*, e70231. [CrossRef]
24. Attallah, O. Deep Learning-Based Model for Paddy Diseases Classification by Thermal Infrared Sensor: An Application for Precision Agriculture. *ISPRS Ann. Photogramm. Remote Sens. Spat. Inf. Sci.* **2023**, *10*, 779.
25. Yang, C.Y.; Zhang, Y.C.; Hou, Y.L. Assessing Water Status in Rice Plants in Water-Deficient Environments Using Thermal Imaging. *Bot. Stud.* **2025**, *66*, 6. [CrossRef] [PubMed]
26. Sharma, D.; Dutta, B.K.; Singh, A.B.; Shome, B.R. Aerobiological, Biochemical and Immunological Studies on Some of the Dominant Aspergillus Species of South Assam (India). *Aerobiologia* **2007**, *23*, 201–210. [CrossRef]
27. Hunter, B.B.; Barnett, H.L. *Illustrated Genera of Imperfect Fungi*, 4th ed.; APS Press: St. Paul, MN, USA, 1998.
28. IRRI. *Standard Evaluation System for Rice*; International Rice Research Institute: Manila, Philippines, 2002; Volume 11.
29. Jia, X.; Yin, D.; Bai, Y.; Yu, X.; Song, Y.; Cheng, M.; Liu, S.; Bai, Y.; Meng, L.; Liu, Y.; et al. Monitoring Maize Leaf Spot Disease Using Multi-Source UAV Imagery. *Drones* **2023**, *7*, 650. [CrossRef]
30. Ji, S.; Gu, C.; Xi, X.; Li, B.; Tan, C.; Zhang, Z.; Hong, Q.; Huo, Z.; Zhao, H.; Zhang, R. Quantitative Monitoring of Leaf Area Index in Rice Based on Hyperspectral Feature Bands and Ridge Regression Algorithm. *Remote Sens.* **2022**, *14*, 2777. [CrossRef]
31. Quille-Mamani, J.; Ramos-Fernández, L.; Huanuqueño-Murillo, J.; Quispe-Tito, D.; Cruz-Villacorta, L.; Pino-Vargas, E.; Flores del Pino, L.; Heros-Aguilar, E.; Ángel Ruiz, L. Rice Yield Prediction Using Spectral and Textural Indices Derived from UAV Imagery and Machine Learning Models in Lambayeque, Peru. *Remote Sens.* **2025**, *17*, 632. [CrossRef]
32. Wang, A.; Song, Z.; Xie, Y.; Hu, J.; Zhang, L.; Zhu, Q. Detection of Rice Leaf SPAD and Blast Disease Using Integrated Aerial and Ground Multiscale Canopy Reflectance Spectroscopy. *Agriculture* **2024**, *14*, 1471. [CrossRef]
33. Panek, E.; Gozdowski, D.; Stępień, M.; Samborski, S.; Ruciński, D.; Buszke, B. Within-Field Relationships between Satellite-Derived Vegetation Indices, Grain Yield and Spike Number of Winter Wheat and Triticale. *Agronomy* **2020**, *10*, 1842. [CrossRef]
34. Guan, Y.; Grote, K. Assessing the Potential of UAV-Based Multispectral and Thermal Data to Estimate Soil Water Content Using Geophysical Methods. *Remote Sens.* **2024**, *16*, 61. [CrossRef]
35. Feng, S.; Jiang, S.; Huang, X.; Zhang, L.; Gan, Y.; Wang, L.; Zhou, C. Detection of Rice Leaf Folder in Paddy Fields Based on Unmanned Aerial Vehicle-Based Hyperspectral Images. *Agronomy* **2024**, *14*, 2660. [CrossRef]
36. Mandal, N.; Adak, S.; Das, D.K.; Sahoo, R.N.; Mukherjee, J.; Kumar, A.; Chinnusamy, V.; Das, B.; Mukhopadhyay, A.; Rajashekara, H.; et al. Spectral Characterization and Severity Assessment of Rice Blast Disease Using Univariate and Multivariate Models. *Front. Plant Sci.* **2023**, *14*, 1067189. [CrossRef] [PubMed]
37. Arumugam Gopalakrishnan, M.; Chellappan, G.; Patil, S.G.; Rathod, S.; Ayyanar, K.; Ramasamy, J.; Nagaranai Karuppasamy, S.; Swaminathan, M. Climate-Based Prediction of Rice Blast Disease Using Count Time Series and Machine Learning Approaches. *AgriEngineering* **2024**, *6*, 4353–4371. [CrossRef]

38. Pisner, D.A.; Schnyer, D.M. Chapter 6—Support Vector Machine. In *Machine Learning: Methods and Applications to Brain Disorders*; Academic Press (AP): London, UK, 2020.
39. Breiman, L. Random forests. *Mach. Learn.* **2001**, *45*, 5–32. [CrossRef]
40. Zhou, Z.; Qiu, C.; Zhang, Y. A Comparative Analysis of Linear Regression, Neural Networks and Random Forest Regression for Predicting Air Ozone Employing Soft Sensor Models. *Sci. Rep.* **2023**, *13*, 22420. [CrossRef] [PubMed]
41. Salman, H.A.; Kalakech, A.; Steiti, A. Random Forest Algorithm Overview. *Babylon. J. Mach. Learn.* **2024**, *2024*, 69–79. [CrossRef] [PubMed]
42. Wang, Y.; Xing, M.; Zhang, H.; He, B.; Zhang, Y. Rice False Smut Monitoring Based on Band Selection of UAV Hyperspectral Data. *Remote Sens.* **2023**, *15*, 2961. [CrossRef]
43. Duarte-Carvajalino, J.M.; Alzate, D.F.; Ramirez, A.A.; Santa-Sepulveda, J.D.; Fajardo-Rojas, A.E.; Soto-Suárez, M. Evaluating Late Blight Severity in Potato Crops Using Unmanned Aerial Vehicles and Machine Learning Algorithms. *Remote Sens.* **2018**, *10*, 1513. [CrossRef]
44. Terentev, A.; Dolzhenko, V.; Fedotov, A.; Eremenko, D. Current State of Hyperspectral Remote Sensing for Early Plant Disease Detection: A Review. *Sensors* **2022**, *22*, 757. [CrossRef] [PubMed]
45. Liu, Z.-Y.; Huang, J.-F.; Tao, R.-X. Characterizing and Estimating Fungal Disease Severity of Rice Brown Spot with Hyperspectral Reflectance Data. *Rice Sci.* **2008**, *15*, 232–242. [CrossRef]
46. Clevers, J.G.P.W.; Gitelson, A.A. Remote Estimation of Crop and Grass Chlorophyll and Nitrogen Content Using Red-Edge Bands on Sentinel-2 and -3. *Int. J. Appl. Earth Obs. Geoinf.* **2013**, *23*, 344–351. [CrossRef]
47. Samsuddin Sah, S.; Abdul Maulud, K.N.; Sharil, S.; Karim, O.A.; Pradhan, B. Monitoring of Three Stages of Paddy Growth Using Multispectral Vegetation Index Derived from UAV Images. *Egypt. J. Remote Sens. Space Sci.* **2023**, *26*, 989–998. [CrossRef]
48. Zhang, D.; Zhou, X.; Zhang, J.; Lan, Y.; Xu, C.; Liang, D. Detection of Rice Sheath Blight Using an Unmanned Aerial System with High-Resolution Color and Multispectral Imaging. *PLoS ONE* **2018**, *13*, e0187470. [CrossRef] [PubMed]
49. Vishwakarma, S.K.; Manzar, N.; Kashyap, A.S. A Systematic Approach for the Detection and Management of Rice Brown Spot Disease. In *Detection, Diagnosis and Management of Air-Borne Diseases in Agricultural Crops*; Springer: Singapore, 2025. [CrossRef]
50. Singh, U.B.; Kumar, R.; Singh, G.P.; Singh, H.B. *Detection, Diagnosis and Management of Air-Borne Diseases in Agricultural Crops*; Springer: Singapore, 2025. [CrossRef]
51. Peñuelas, J.; Gamon, J.A.; Griffin, K.L.; Field, C.B. Assessing Community Type, Plant Biomass, Pigment Composition, and Photosynthetic Efficiency of Aquatic Vegetation from Spectral Reflectance. *Remote Sens. Environ.* **1993**, *46*, 110–118. [CrossRef]
52. Mirandilla, J.R.F.; Yamashita, M.; Yoshimura, M.; Paringit, E.C. Leaf Spectral Analysis for Detection and Differentiation of Three Major Rice Diseases in the Philippines. *Remote Sens.* **2023**, *15*, 3058. [CrossRef]
53. Saeed, M.; Kim, J.S.; Kim, S.Y.; Ryu, J.E.; Ko, J.H.; Zaidi, S.F.A.; Seo, J.A.; Kim, Y.S.; Lee, D.Y.; Choi, H.K. Differentiation of Geographical Origin of White and Brown Rice Samples Using NMR Spectroscopy Coupled with Machine Learning Techniques. *Metabolites* **2022**, *12*, 1012. [CrossRef] [PubMed]
54. Liu, X.; Gao, C.; Li, P. A Comparative Analysis of Support Vector Machines and Extreme Learning Machines. *Neural Netw.* **2012**, *33*, 58–66. [CrossRef] [PubMed]
55. Tripathi, R.; Gouda, A.K.; Jena, S.S.; Mohapatra, R.R.; Lal, M.K.; Dash, S.K.; Sahoo, R.N.; Nayak, A.K. Rice Yield Prediction Using UAV-Mounted RGB Sensors and Machine Learning Algorithms. *Proc. Indian Natl. Sci. Acad.* **2025**, 1–16. [CrossRef]
56. Berger, K.; Machwitz, M.; Kycko, M.; Kefauver, S.C.; Van Wittenberghe, S.; Gerhards, M.; Verrelst, J.; Atzberger, C.; van der Tol, C.; Damm, A.; et al. Multi-Sensor Spectral Synergies for Crop Stress Detection and Monitoring in the Optical Domain: A Review. *Remote Sens. Environ.* **2022**, *280*, 113198. [CrossRef] [PubMed]